Silicate minerals and Si-O glass in comet Wild 2 samples: Transmission electron microscopy

Kazushige TOMEOKA*, Naotaka TOMIOKA, and Ichiro OHNISHI

Department of Earth and Planetary Sciences, Faculty of Science, Kobe University, Nada, Kobe 657-8501, Japan
*Corresponding author. E-mail: tomeoka@kobe-u.ac.jp

Abstract–A transmission electron microscope (TEM) study of seven comet Wild 2 samples shows that three samples consist mainly of olivine and pyroxene and four samples consist of Mg-Fe-bearing Si-O glass with minor amounts of Fe-Ni sulfide and metal. The olivine in the silicate-rich samples differs in fayalite content between the samples and shows a wide range of fayalite content within individual samples, indicating that the degree of thermal metamorphism on the comet, if any, was extremely low. One olivine grain has a high density of dislocations with Burgers vector $b = [001]$, suggesting that the Wild 2 particles experienced hypervelocity impacts before capture. The structural type and composition of pyroxene differ between the samples and within individual samples. Both low-Ca and high-Ca pyroxenes are present. Enstatite occurs as ortho- and clinoenstatite, suggesting that the Wild 2 particles contain materials that went through distinct high-temperature and cooling histories.

One silicate-rich sample exhibits a zone texture consisting of a core of low-Ca pyroxene surrounded by an inner rim of Mg-Fe-bearing Si-O-rich glass and an outer rim of melted aerogel. The texture suggests that the inner rim was formed by the mixing of melted cometary low-Ca pyroxene and melted aerogel during capture heating.

The four Mg-Fe-bearing, Si-O glass–rich samples show close similarities in mineralogy and texture to the inner rim of the zoned silicate-rich sample. The four samples are probably secondary products formed by interaction between melted cometary silicates and melted aerogel during the capture process.

INTRODUCTION

Comet Wild 2 particles collected by the Stardust mission were successfully returned to Earth on 15 January 2006. Shortly after, the returned samples were distributed to investigators around the world for the preliminary analysis (Brownlee et al. 2006). We received nine Wild 2 samples from NASA Johnson Space Center (JSC) during the period of February 2006 to June 2006 (Table 1). This paper summarizes our mineralogical investigation of those nine samples using a transmission electron microscope (TEM). Some of our earlier results have been published as part of a comprehensive summary of the preliminary analysis (Zolensky et al. 2006). Our results reveal that the nine samples can be divided into three groups based on their constituent minerals: 1) crystalline silicate-rich (three samples), 2) Si-O glass–rich (four samples), and 3) nondefinable (two samples) (Table 1). All three samples in group (1) were identified at track termini in the aerogel capture cells, whereas the remainder was found along tracks. This paper focuses on the results of the samples

in groups (1) and (2). The two samples in group (3) contain unusual materials, some of which may be contaminants; they are described in the Appendix.

The goal of our study was to provide the mineralogical and chemical details of the Wild 2 samples, to determine the extent to which, and how, the particles were modified by interaction with aerogel during the capture process, and to clarify the true nature of the cometary particles. We also intended to compare the mineralogy and chemistry of the cometary particles with those of primitive meteorites and interplanetary dust particles (IDPs), and to unravel the formation history of the cometary particles and the physical and chemical processes that could have taken place in the comet.

MATERIALS AND METHODS

The Wild 2 samples studied are ultramicrotomed sections (70–100 nm thick) mounted on amorphous C-supported Cu TEM grids. They were prepared at NASA

Table 1. Wild 2 samples studied and size of major aggregates on TEM grids.

Sample no.	Aggregate size (µm)
Silicate-rich samples	
FC13-0-17-1-3	11.3 × 7.5
	8.2 × 4.3
	5.3 × 3.7
C2115-24-22-1-8	20.0 × 2.9
	7.5 × 2.3
	2.6 × 0.9
	2.1 × 0.9
	1.6 × 1.6
C2027-2-69-1-4	14.4 × 8.1
	13.1 × 8.8
Si-O glass-rich samples	
C2054-0-35-16-6*	12.5 × 7.2
	4.9 × 0.7
	4.0 × 2.7
	1.1 × 0.2
C2054-0-35-44-3*	14.5 × 8.0
	12.5 × 8.5
C2054-0-35-53-3*	9.2 × 3.8
	8.9 × 4.2
	1.5 × 0.9
C2004-1-44-4-4	23.0 × 11.0
	18.5 × 4.8
Nondefinable samples	
FC4-0-3-1-1	4.3 × 3.8
	3.8 × 3.4
	3.1 × 2.5
	3.3 × 2.3
	2.8 × 2.3
	2.6 × 1.5
FC12-0-16-1-6	3.8 × 1.3

The three silicate-rich samples are from track termini. The remainder is from track walls. *From the same track, Track 35.

JSC. Details of the sample preparation are described in Zolensky et al. (2006).

The microstructure and composition of minerals in the thin sections were investigated using a JEM-2010 TEM, operated at 200 kV and equipped with an energy dispersive X-ray spectrometer (EDS, Noran Voyager). Structural identification was based on selected-area electron diffraction (SAED). For the initial observations, a relatively broad electron beam (1–4 µm in diameter) was used to obtain compositional information from large areas. Chemical analysis of individual minerals was performed using a finely focused beam (20–200 nm in diameter). Quantitative chemical data were derived for specific minerals using thin film X-ray microanalysis techniques. For quantitative microanalysis, terrestrial olivine, pyroxene, and K-feldspar were used as reference standards for the major elements in silicate minerals, and pyrite was used for Fe and S in sulfides. The Ni content was determined using SUS316 stainless steel as a standard.
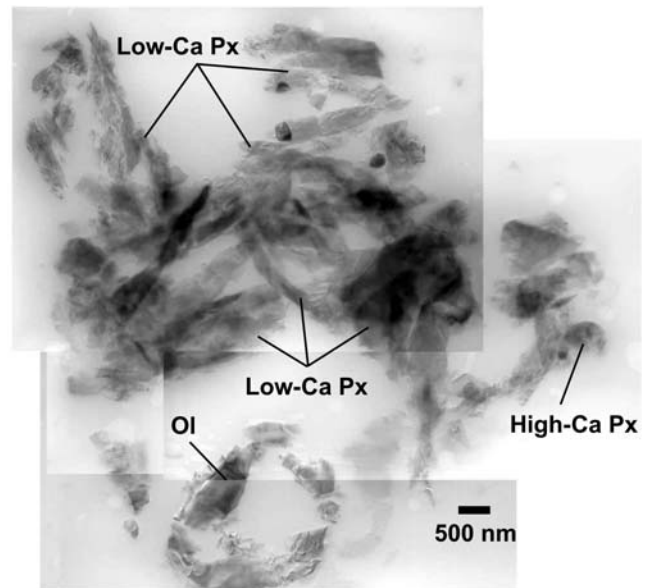

Fig. 1. Low-magnification TEM image of an aggregate of Sample FC13-0-17-1-3, consisting of grains of low-Ca pyroxene (Px), olivine (Ol), and high-Ca pyroxene. The interspaces between the silicate grains are filled with Si-O glass.

Ultramicrotomed sections of the Wild 2 samples on the TEM grids consist of one to six major aggregates, and minor amounts of smaller aggregates and fine grains. Our TEM study focused on the major aggregates. The number and size of the major aggregates in each sample are listed in Table 1.

RESULTS

Silicate-Rich Samples

FC13-0-17-1-3

The aggregates on the TEM grid consist of lath-shaped, anhedral to euhedral grains (0.3–1.5 µm in size) of low-Ca pyroxene and minor amounts of anhedral grains (0.5–1.0 µm) of olivine (Figs. 1, 2a, and 2b). High-Ca pyroxene also occurs as anhedral grains (0.2–0.5 µm) in a lower abundance (Fig. 2c). The interspaces between the grains are filled with Si-O-rich glass. Broad-beam EDS analysis of the aggregates shows that their bulk composition is characterized by major amounts of Si, O, and Mg and minor amounts of Fe and Ca (Fig. 3a), reflecting the predominant occurrence of low-Ca pyroxene and interstitial Si-O-rich glass. The SAED patterns from the low-Ca pyroxene grains indicate that they are orthorhombic pyroxene (orthopyroxene) (Fig. 2a). Minor amounts of anhedral grains (0.1–0.3 µm in diameter) of Ni-bearing Fe sulfide are scattered about the aggregates (Fig. 2d).

The low-Ca pyroxene has a variable Fe/(Fe + Mg) ratio, ranging mostly from Fs_3 to Fs_{13}, with Wo_{1-5} (Fig. 4), which is in the range of enstatite. It contains minor, variable amounts of Al, Cr, and Mn. The high-Ca pyroxene has a composition range from Fs_{15} to Fs_{19} and from Wo_{34} to Wo_{38} (Fig. 4),
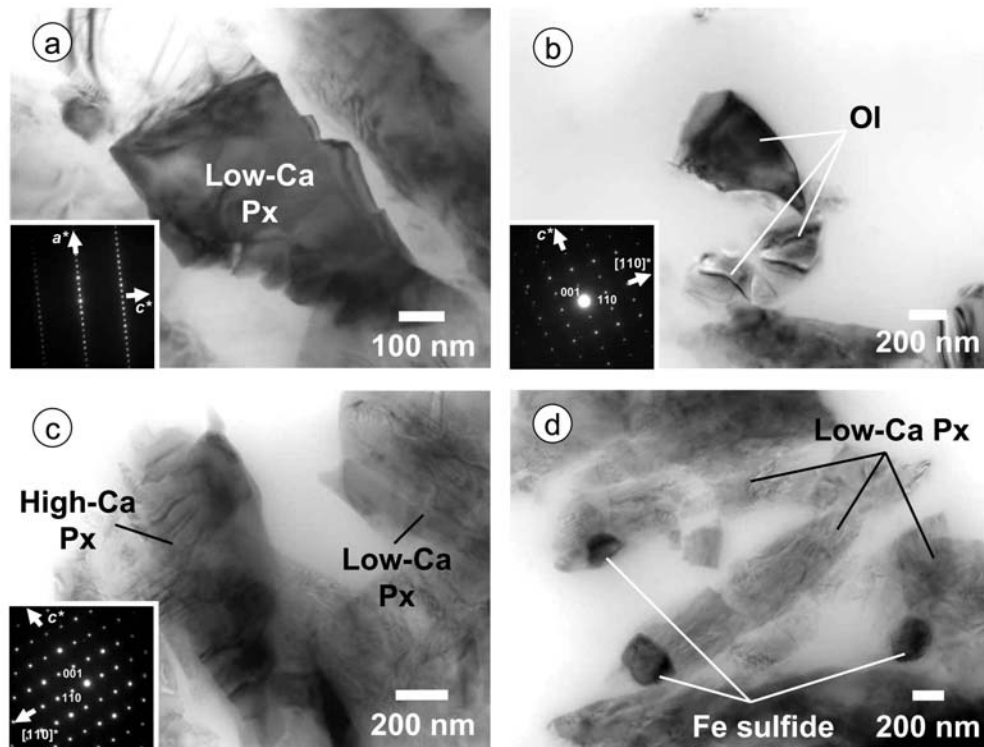
Fig. 2. TEM images of mineral grains in Sample FC13-0-17-1-3. a) A low-Ca pyroxene (Px, orthoenstatite) grain having a somewhat euhedral shape, viewed along [010]. In the inset is its SAED pattern. b) Olivine (Ol) grains. In the inset is an SAED pattern from the largest olivine grain in the image. c) A high-Ca pyroxene (Px) grain and a low-Ca pyroxene grain. In the inset is an SAED pattern from the high-Ca pyroxene grain. d) Ni-bearing Fe-sulfide grains with low-Ca pyroxene grains. Note that the sulfide grains are anhedral and large in size compared with the Fe-Ni-S inclusions in the other samples (see Fig. 12b, 13, 14a, and 14b).

corresponding to augite. The olivine is also variable in its Fe/(Fe + Mg) ratio, ranging from Fa_{30} to Fa_{50} (Fig. 5a). The Fa content is higher relative to the olivine in most other reported Wild 2 samples (Fig. 5d). Olivine contains minor, variable amounts of Mn. The Fe sulfide grains are homogeneous in composition and close to stoichiometric FeS with <3 atomic% Ni (Fig. 6a).

C2115-24-22-1-8

These aggregates consist of lath-shaped to anhedral grains (0.2 to 2.0 μm in size) of olivine and less abundant high-Ca pyroxene and Si-O-Al-rich glass (Figs. 7a and 7b). The high-Ca pyroxene grains are commonly polycrystalline (Fig. 8a). The Si-O-Al-rich glass occurs as irregularly shaped discrete grains (0.3 to 1.0 μm in size, Figs. 7 and 8b). This occurrence differs from that of the interstitial Si-O-rich glass in Sample FC13-0-17-1-3. Neither metal nor sulfide is present. Broad-beam EDS analysis of the aggregates shows that their bulk composition is similar to the chondritic composition, except that both S and Ni are absent (Fig. 3b).

The olivine exhibits a very wide compositional range, from Fa_9 to Fa_{36} (Fig. 5b). It contains minor, variable amounts of Mn. Olivine grains within individual aggregates show slightly but distinct compositions (Figs. 7a and 7b), exhibiting a wide range of compositional heterogeneity on the submicron scale. In comparison, the high-Ca pyroxene is homogeneous in composition, and

close to diopside, with Fs_{9-12} (Fig. 4). It contains minor, variable amounts of Cr, Na, and Al. The Si-O-Al-rich glass contains minor, variable amounts of Na, Mg, and K (Fig. 8c).

One of the olivine grains exhibits a characteristic texture resulting from a high density of dislocations (Fig. 9). The dislocations have Burgers vector $b = [001]$ and long segments in the [001] screw orientation. The density of the dislocations is in the order of 10^{10} cm^{-2}. Such a high density of dislocations of this type is known to be diagnostic of deformation at high strain rates and low temperatures (e.g., Ashworth and Barber 1975; Ashworth 1985), and is most likely a result of shock deformation. The microtexture exactly matches those found in shocked ordinary and carbonaceous chondrites (Ashworth 1985; Nakamura et al. 1992; Langenhorst et al. 1995; Joreau et al. 1997) and an experimentally shocked ordinary chondrite (Sears et al. 1984).

C2027-2-69-1-4

These aggregates have partially smooth, somewhat rounded external shapes and exhibit a zone texture consisting of a core surrounded by inner and outer rims (Fig. 10).

The core consists of an aggregate of lath-shaped to anhedral grains (0.5–2.0 μm in size) of Fe-bearing low-Ca pyroxene with Fs_{20-32} and Wo_{3-9} (Fig. 4). The composition ranges from enstatite to pigeonite. The SAED patterns from the pyroxene grains indicate that they are monoclinic pyroxene (clinopyroxene) with a
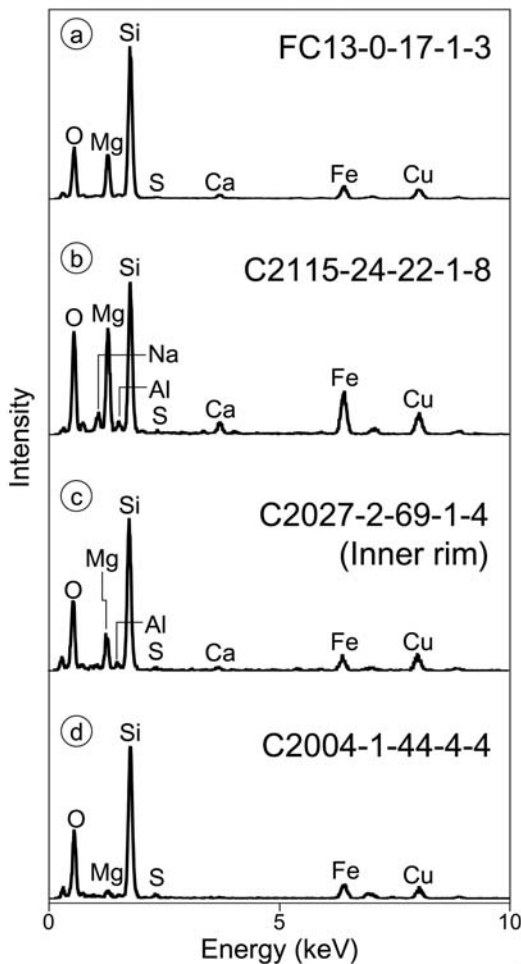
Fig. 3. Broad-beam EDS spectra from Sample FC13-0-17-1-3 (Silicate-rich type) (a), Sample C2115-24-22-1-8 (Silicate-rich type) (b), the inner rim of Sample C2027-2-69-1-4 (Silicate-rich type) (c), and Sample C2004-1-44-4-4 (Si-O glass-rich type) (d). Cu peaks are from the TEM grids.
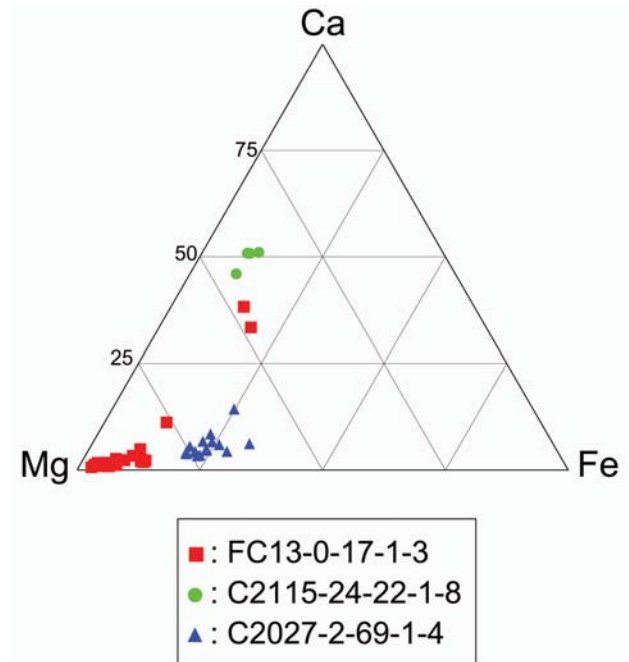

Fig. 4. A plot of analyses of pyroxenes in the three silicate-rich Wild 2 samples (atomic%).
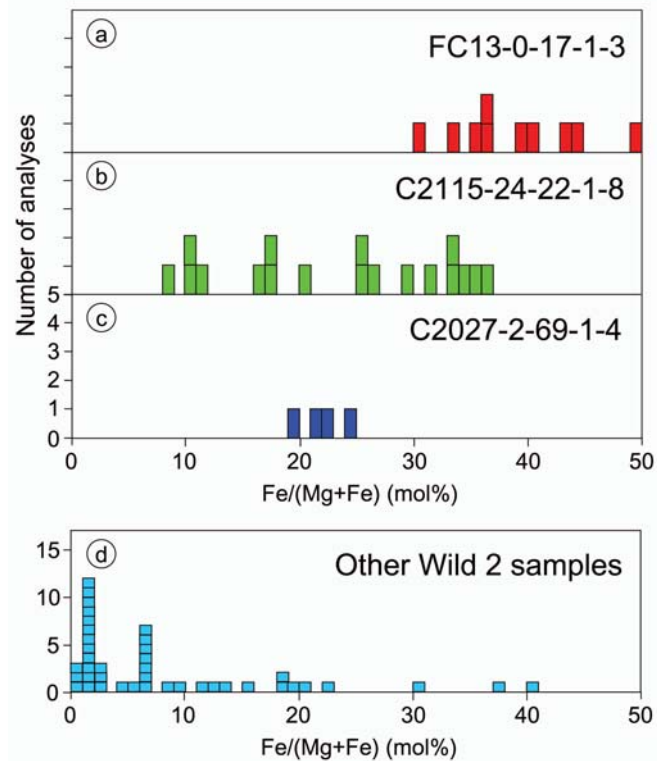

Fig. 5. Composition ranges of olivines in the three silicate-rich Wild 2 samples, FC13-0-17-1-3 (a), C2115-24-22-1-8 (b), C2027-2-69-1-4 (c), and other Wild 2 samples (d) (data from Zolensky et al. 2006).

disordered stacking of ortho- and clinopyroxene (Fig. 11a). Some of the pyroxene grains are polycrystalline. The pyroxenes contain minor, variable amounts of Al and Cr. Olivine occurs in very minor amounts, as small subrounded to anhedral grains (0.2–0.4 μm in size) that form aggregates with low-Ca pyroxene grains with a similar size and shape (Fig. 11b). The olivine has a composition range of Fa_{19} to Fa_{24}.

The inner rim consists of an array of plates (0.2–0.3 μm in width and 0.5–2.0 μm in length) that are oriented in approximately the same direction (Figs. 10, 12a, and 12b). The plates are composed of Si-O glass containing minor, variable amounts of Mg and Fe, and lesser, variable amounts of Ca and Al (Fig. 3c). The plates have a smooth appearance, but in places, contain high densities of Fe-Ni-S inclusions (5–150 nm in diameter) and vesicles (10–300 nm in diameter) (Figs. 12a and 12b). The Fe-Ni-S inclusions are commonly spherical in shape, suggesting that they are melted droplets (Fig. 12b). There are two main types of Fe-
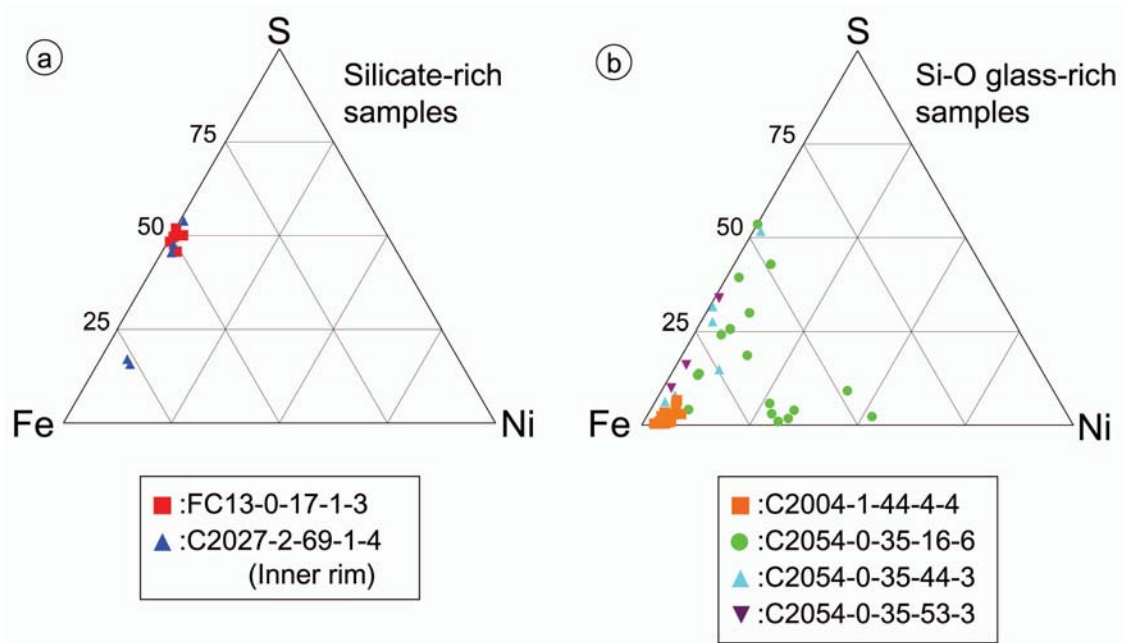
Fig. 6. Plots of analyses of Fe-Ni-S inclusions from the two silicate-rich samples (a) and the four Si-O glass-rich samples (b) (atomic%). The analyses were obtained from relatively large inclusions (>100 nm in diameter).
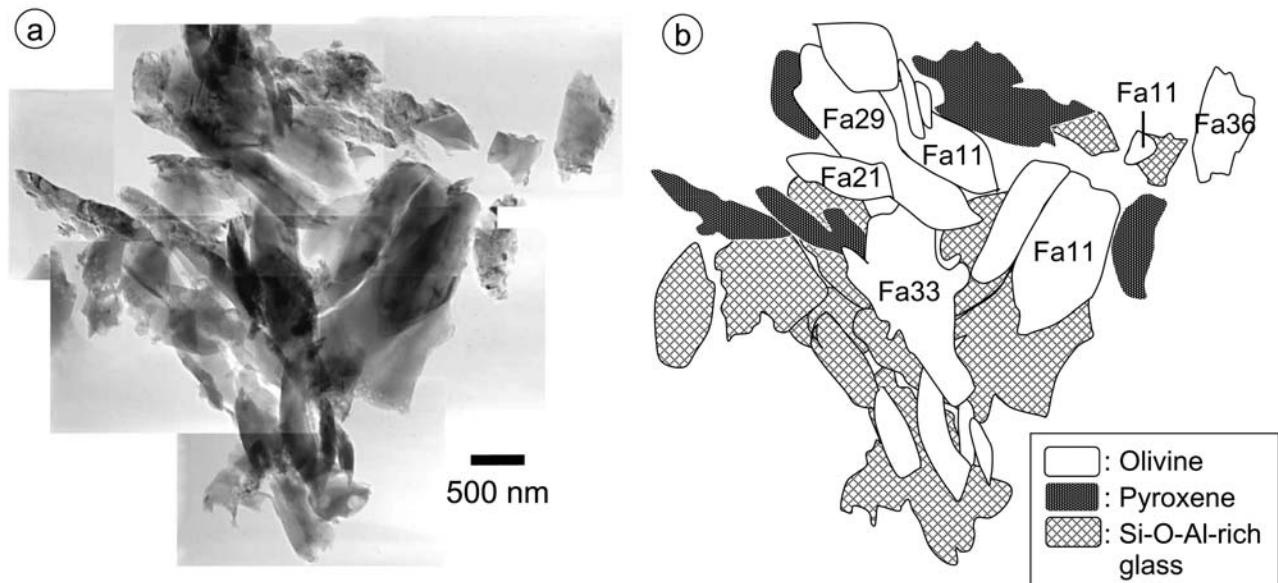

Fig. 7. a) Low-magnification TEM image of an aggregate of Sample C2115-24-22-1-8. b) Illustration of the aggregate in (a) showing grains of olivine, high-Ca pyroxene, and Si-O-Al-rich glass. Fayalite (Fa) contents of olivine grains are indicated.

Ni-S inclusions: one has a composition close to FeS, and the other has an intermediate composition between FeS and Fe (Fig. 6a), which is probably a mixture of Fe-Ni sulfide and metal.

The outer rim consists of aggregates of extremely small globules of Si-O glass (10–100 nm in diameter) (Fig. 12a) that contains no other elements. These globules are probably melted aerogel.

Si-O Glass-Rich Samples

Samples C2004-1-44-4-4, C2054-0-35-16-6, C2054-0-35-44-3, and C2054-0-35-53-3 (Table 1) show a close similarity in their mineralogy and texture. Thus, we focus on the data from Sample C2004-1-44-4-4, which is the largest of the four samples. Sample C2004-1-44-4-4 was extracted from track 44, which is the largest impact
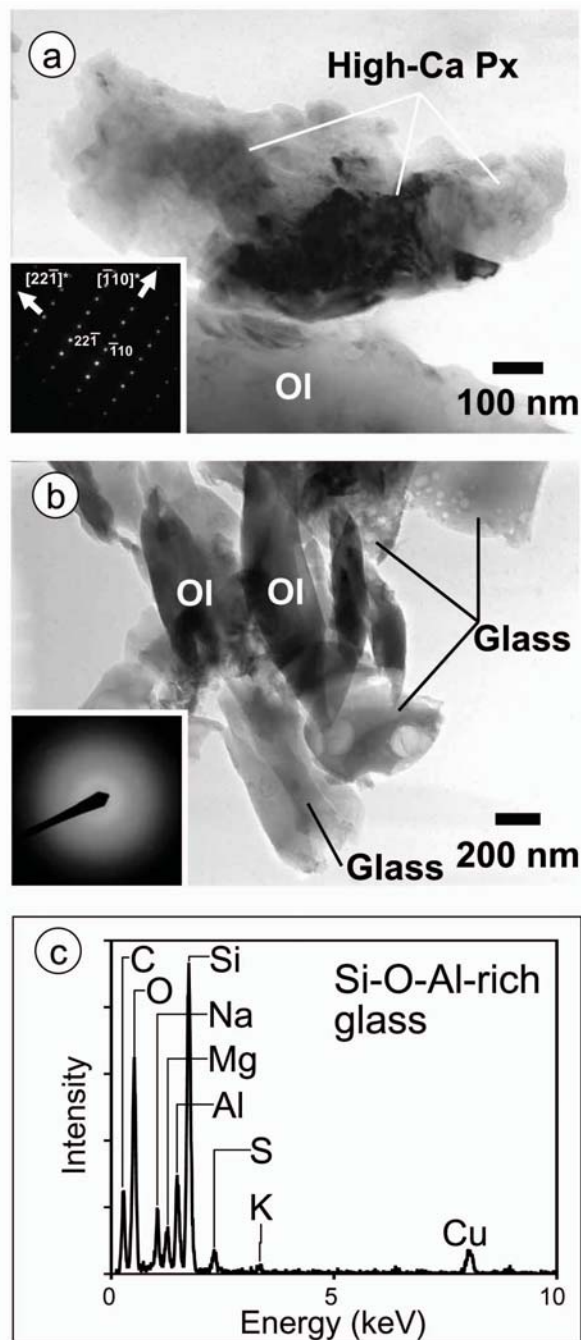
Fig. 8. a) TEM image of a polycrystalline grain of high-Ca pyroxene (diopside) in Sample C2115-24-22-1-8. In the inset is an SAED pattern from the darkest area in the grain. b) TEM image of grains of olivine (Ol) and Si-O-Al-rich glass (Glass). In the inset is an SAED pattern from an Si-O-Al-rich glass grain showing no diffraction spots. c) EDS spectrum from the Si-O-Al-rich glass. A Cu peak is from the TEM grid. A S peak is probably from a residue of the embedding medium.

feature in the cometary tray. It is large because the cometary particle struck the edge of the tray frame and then bounced into the adjacent aerogel (from the Stardust Catalog). Samples C2054-0-35-16-6, C2054-0-35-44-3

and C2054-0-35-53-3 were extracted from the wall of the same track, track 35.

The aggregates of Sample C2004-1-44-4-4 on the TEM grid consist of arrays of approximately parallel-oriented plates that have dimensions of 0.1–0.4 μm in width and 0.5–3.0 μm in length (Fig. 13). This texture is largely an artifact caused by the ultramicrotome slicing, and thus, before slicing, individual aggregates probably constituted a single more massive, coherent grain (or grains). Broad-beam EDS analysis of the aggregates shows that their bulk composition is dominated by Si and O, with minor amounts of Mg, Fe, and S (Fig. 3d). The plates have a smooth appearance, and consist of Si-O glass containing minor variable amounts of Mg and Fe. Lesser, variable amounts of Ca and Al are also detected. In places, the plates contain numerous spherical Fe-Ni-rich inclusions (5–300 nm in diameter) and vesicles (20–300 nm) (Figs. 13 and 14a). A relatively large Fe-Ni-rich inclusion (~230 nm in diameter) exhibits an SAED pattern corresponding to kamacite (Fig. 14b). The SAED patterns from areas with high concentrations of smaller inclusions exhibit a diffraction ring at d = 0.20 nm corresponding to the strongest (110) reflection of kamacite (Fig. 14a). Thus, we identify most of the Fe-Ni-rich inclusions to be kamacite. The kamacite contains <8 atomic% of Ni. The inclusions occasionally contain minor amounts of S, which probably come from Fe sulfide mixed with kamacite.

Noteworthy differences between the four Si-O glass-rich samples are observed in the compositions of the Fe-Ni-S inclusions. EDS analyses of the Fe-Ni-S inclusions in the four samples are plotted in terms of their Fe, Ni, and S contents in Figure 6b. Analyses of most of the inclusions in Sample C2004-1-44-4-4 are concentrated near the Fe apex, being consistent with our identification that they are kamacite. The inclusions in Samples C2054-0-35-44-3 and C2054-0-35-53-3 contain more abundant Fe sulfide than those in Sample C2004-1-44-4-4. Compared to the inclusions in these three samples, the inclusions in Sample C2054-0-35-16-6 contain distinctly more variable amounts of Ni-rich metal, which is probably taenite.

DISCUSSION

Mineralogical Characteristics of the Silicate-Rich Samples

The results of our study reveal that the three samples, FC13-0-17-1-3, CC2115-24-22-1-8, and C2027-2-69-1-4, consist mainly of crystalline silicates (Table 2). To evaluate the significance of their mineralogical characteristics, an important question to be addressed is to what extent those particles have been altered during the capture process. Zolensky et al. (2006) proposed that loss of S from Fe-Ni sulfides is a result of capture heating, and can be used to estimate the degree of modification during capture of the host Wild 2 particles. Using this criterion, Sample FC13-0-17-1-3 probably escaped any significant heating, because all the

Table 2. Silicates and sulfide/metal in the silicate-rich samples.[a]

Sample	Olivine	Low-Ca pyroxene	High-Ca pyroxene	Sulfide/Metal
FC13-0-17-1-3	Fa_{30-50}	$Fs_{3-13}Wo_{1-5}$ (Oen)	$Fs_{15-19}Wo_{34-38}$ (Aug)	Fe(Ni)S
C2115-24-22-1-8	Fa_{9-36}	–	$Fs_{9-12}Wo_{46-51}$ (Di)	–
C2027-2-69-1-4	Fa_{19-24}	$Fs_{20-32}Wo_{3-9}$ (Cen-Pig)	–	Fe(Ni)S–Fe(Ni)

[a]Fa = fayalite, Fs = ferrosilite, Wo = wollastonite, Oen = orthoenstatite, Cen = clinoenstatite, Pig = pigeonite, Aug = augite, Di = diopside.
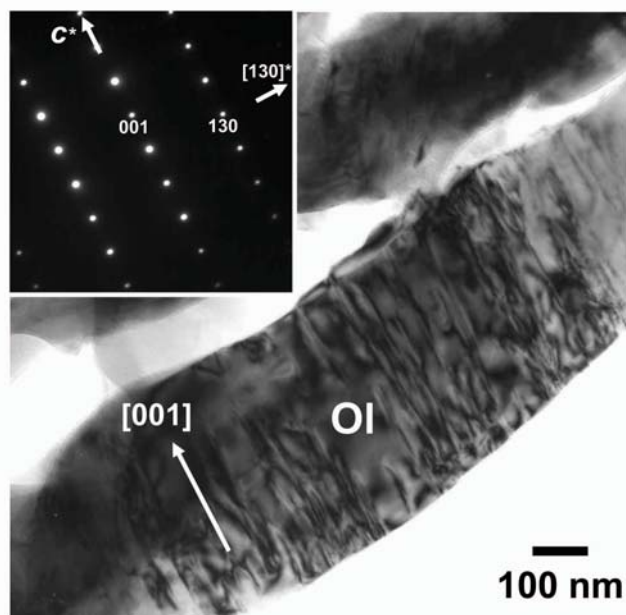

Fig. 9. TEM image of an olivine grain having a high density of dislocations with straight, long segments in the [001] screw orientation, and its SAED pattern (inset), from Sample C2115-24-22-1-8.

sulfide grains show a composition close to stoichiometric FeS (Fig. 6a). In addition, the sulfide grains are anhedral and relatively larger than the Fe-Ni-S inclusions in the other samples, suggesting that they have not been melted. Sample C2115-24-22-1-8 contains neither sulfide nor metal, and thus, the criterion cannot be applied. In contrast to Sample FC13-0-17-1-3, Sample C2027-2-69-1-4 contains Fe-Ni sulfide that has apparently been melted and mixed with metal, indicating that this sample went through significant heating.

Olivine

The olivine in the three silicate-rich samples differs in its Fa content, and shows a wide range of Fa content within individual samples (Figs. 5a–5c). The range of composition is comparable to that in anhydrous chondritic IDPs, and some unequilibrated chondrites (Zolensky et al. 2006; Brearley and Jones 1998). In chondrites, the Fa content in olivine is related to the degree of thermal metamorphism that took place on the meteorite parent body. The composition of olivine in chondrites becomes progressively more equilibrated, because of the diffusive exchange of Mg and Fe, as a function of increasing degree of thermal metamorphism. Thus, the compositional characteristics of olivine in the Wild 2 samples

studied here suggest that it has not been affected by any significant degree of parent-body thermal metamorphism.

It is particularly remarkable that individual olivine grains with a diameter of 0.2–2.0 μm within each aggregate of Sample C2115-24-22-1-8 exhibit a distinct composition ranging from Fa_9 to Fa_{36} (Figs. 7a and 7b). These olivine grains probably constituted a coarser single grain (or grains) before microtome slicing, and thus, the different Fa contents between the olivine grains suggest that the olivine grain (or grains) before slicing was heterogeneous in composition on the submicron scale. Such heterogeneity is most likely explained by chemical zoning. In chondrites, such fine-scale chemical zoning of olivine is observed in the least equilibrated type 3 chondrites (e.g., Jones and Scott 1989; Jones 1990). Therefore, our observations strongly suggest that the degree of thermal metamorphism on comet Wild 2, if any, was extremely low.

The observation of an olivine grain with a high density of dislocations (Fig. 9) provides evidence that the Wild 2 particle has experienced hypervelocity impacts before capture. Based on shock experiments, such high-density dislocations are known to be formed by deformation induced by shock at peak pressures greater than 27 GPa (Sears et al. 1984; Ashworth 1985). In the case of impacts on the aerogel, the shock pressure is significantly lower than on normal rock targets because of its extremely low-density, highly viscous nature. From the calculations of Kitazawa et al. (1999), the shock pressure generated by an impact of an olivine projectile on the aerogel with a density of 0.128 g/cm^3 at a speed of 6.1 km/s (Stardust's encounter speed) is approximately 1 GPa. Because the density of the Stardust aerogel (<0.05 g/cm^3) is less than this value, the pressures generated by impacts on the Stardust aerogel are estimated to be less than 1 GPa. This means that it is reasonable to ascribe the high-density dislocations in the Wild 2 olivine to impacts before capture. The Stardust's encounter with comet Wild 2 in 2004 revealed that the nucleus of the comet has unusual circular features that appear to be impact craters (Brownlee et al. 2004). Our finding of the olivine grain with high-density dislocations may provide evidence that Wild 2 has indeed experienced such impact events.

Pyroxene

Pyroxene occurs in all three samples as the major phase. Its structural type and composition show striking differences, both between samples and within individual
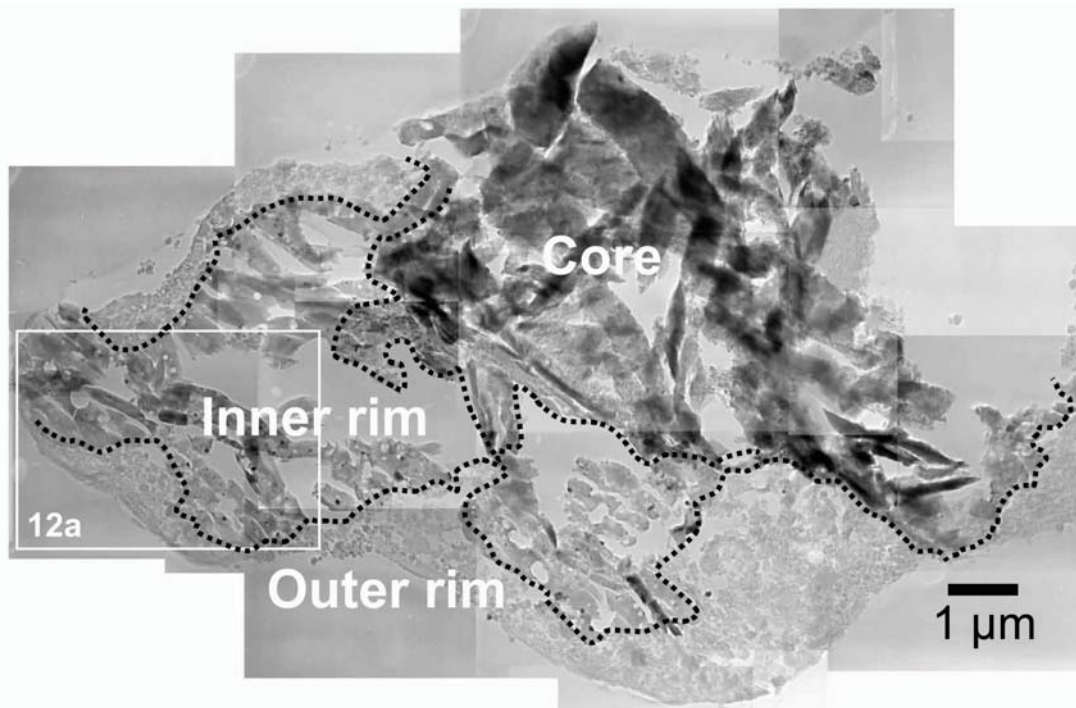
Fig. 10. Low-magnification TEM image of an aggregate of Sample C2027-2-69-1-4, consisting of a core surrounded by an inner rim and an outer rim. An image of the boxed area is shown in Fig. 12a.

samples. The pyroxene occurring in the three samples is listed in Table 2, and its compositions are plotted in terms of the Ca, Mg, and Fe contents in Fig. 4. Although Samples FC13-0-17-1-3 and C2027-2-69-1-4 contain enstatite, the enstatite in the former sample is orthoenstatite, and the enstatite in the latter sample is clinoenstatite. Orthoenstatite is known to form through very slow cooling from temperatures above 600 °C, whereas clinoenstatite forms by rapid cooling from primary protoenstatite that is stable at temperatures above 1000 °C (Smyth 1974; Jiang et al. 2002). Therefore, the difference in the structural type of enstatite suggests that the Wild 2 enstatites experienced distinct high-temperature and cooling histories. However, in regard to the clinoenstatite, we cannot preclude the possibility that it formed through rapid cooling during aerogel capture.

The low-Ca pyroxenes in Samples FC13-0-17-1-3 and C2027-2-69-1-4 differ in their Fs content (or Fe/(Fe + Mg) ratio) and show considerable variation within individual samples (Fig. 4). These variations in Fs content are consistent with the variations in Fa content in the olivine (Figs. 5a and 5c) as discussed above, and further support the interpretation that these samples were thermally unequilibrated.

Si-O-Al-Rich Glass

The olivine-rich Sample C2115-24-22-1-8 contains Si-O-Al-rich glass (Figs. 7 and 8b) with minor variable amounts of Na, Mg, and K (Fig. 8c). The composition is clearly different from melted aerogel, and suggests that it is related to indigenous cometary glass. In chondrites, Al-rich Si-O glass with variable amounts of Ca, Na, Mg, and K occurs in chondrule mesostasis (e.g., Jones and Scott 1989), which resulted from a rapid cooling from the chondrule droplet, after crystallization of Mg-Fe-rich silicates such as olivine and pyroxene. From these observations, we infer that the Si-O-Al-rich glass could be related to chondrule mesostasis, although we cannot exclude the possibility that it was partially mixed with melted aerogel. In chondrule mesostasis, glass commonly includes micron-to-submicron scale quenched crystallites of high-Ca pyroxene (e.g., Brearley and Jones 1998; Tomeoka and Itoh 2004). Thus, the coexistence of the Si-O-Al-rich glass with diopside in Sample C2115-24-22-1-8 supports our inference.

The Core-to-Rim Texture of the Silicate-Rich Sample

The aggregates in Sample C2027-2-69-1-4 were found to have a core-to-rim zone texture (Fig. 10), which provides insight into how the cometary particles were altered by interaction with the surrounding aerogel during capture heating.

The low-Ca pyroxene in the core is probably indigenous cometary pyroxene. The outermost rim consists of Si-O glass that is most likely the result of aerogel melting. On the other hand, the inner rim consists largely of Si-O glass with minor, variable amounts of Mg and Fe (Fig. 3c), having a composition intermediate between the core and the outermost
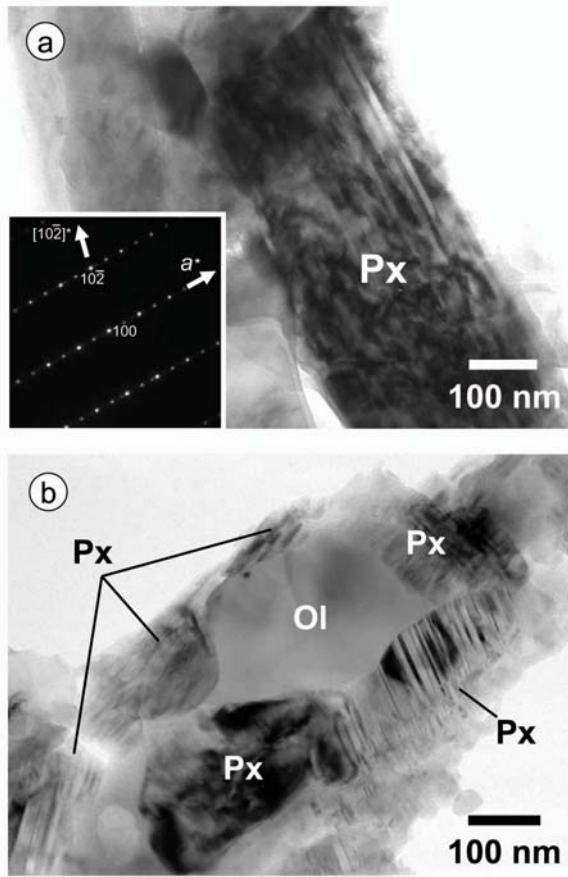
Fig. 11. a) TEM image of a low-Ca pyroxene (clinoenstatite) grain having alternating light and dark bands of varying widths resulting from intimate intergrowths of ortho- and clinoenstatite, from the core of the C2027-2-69-1-4 aggregate. In the inset is its SAED pattern exhibiting diffuse reflections along *a**, indicating a stacking disorder of ortho- and clinoenstatite. b) TEM image of an aggregate of olivine (Ol) and low-Ca pyroxene (Px) grains. One of the pyroxene grains, located on the lower-right side of the olivine grain, shows contrast arising from (100) stacking faults.
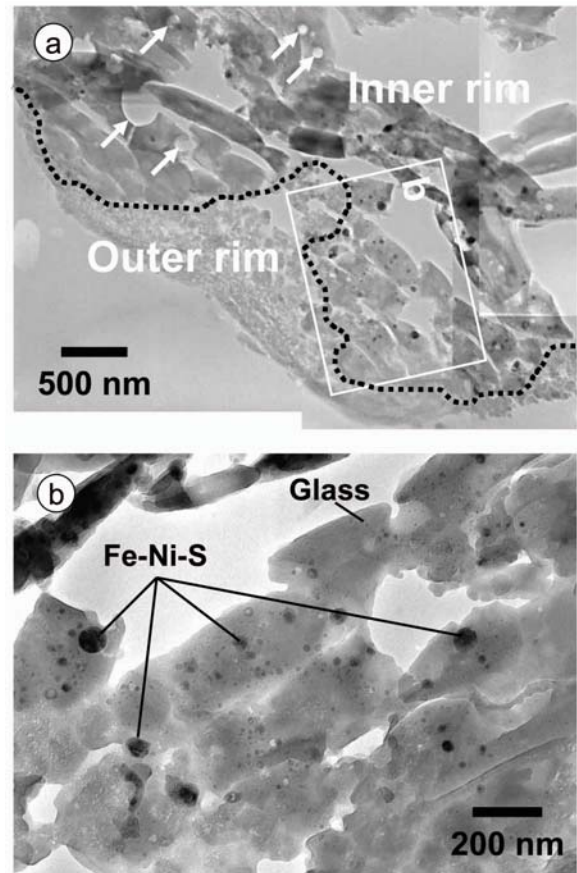

Fig. 12. a) TEM image of the boxed area in Fig. 10, showing the inner rim and the outer rim of the C2027-2-69-1-4 aggregate. Several vesicles in the inner rim are indicated by white arrows. b) Image of the boxed area in (a), showing that the Mg-Fe-bearing Si-O glass (Glass) contains numerous inclusions of Fe-Ni sulfide and metal (Fe-Ni-S).

rim. These textural and compositional characteristics suggest that the Mg-Fe-bearing Si-O glass in the inner rim was formed by a mixing of the melted low-Ca pyroxene and aerogel during capture heating. This implies that the inner rim was heated to a temperature higher than the melting point of the pyroxene (~1300 °C, from Huebner and Turnock [1980]). The Fe-Ni sulfide/metal contained in the incident cometary particle would have been preferentially melted, as a result of their relatively low eutectic point (950 °C, from Kullerud [1963]), and dispersed widely as droplets throughout the inner rim. Simultaneously, vesicles would have been formed from gas contained in the micro-pores in the aerogel, and also from partial volatilization of the sulfur in the sulfide. The heterogeneities in the Mg, Fe, Ca, and Al contents in the inner rim probably reflect differences in the volume proportion of melted pyroxene and aerogel. Therefore, the core-to-rim zone texture in Sample C2027-2-69-1-4 can be regarded as
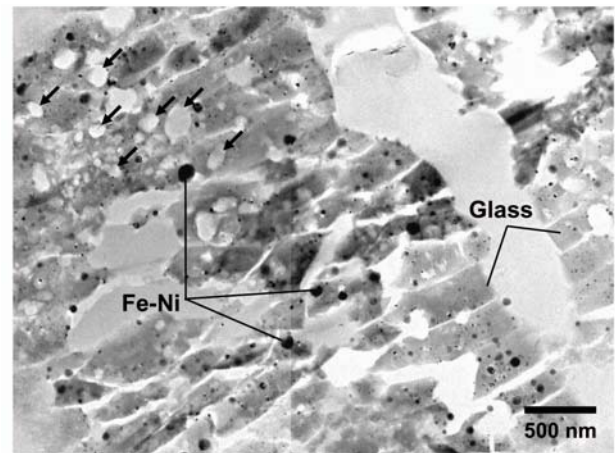

Fig. 13. TEM image of a portion of an aggregate of Sample C2004-1-44-4-4 consisting of parallel-oriented plates of Mg-Fe-bearing Si-O glass (Glass) with a high density of Fe-Ni-rich inclusions (Fe-Ni, dark grains). Most Fe-Ni-rich inclusions are kamacite occasionally mixed with Fe sulfide. The glass also includes a high density of vesicles, several of which are indicated by arrows (top-left).
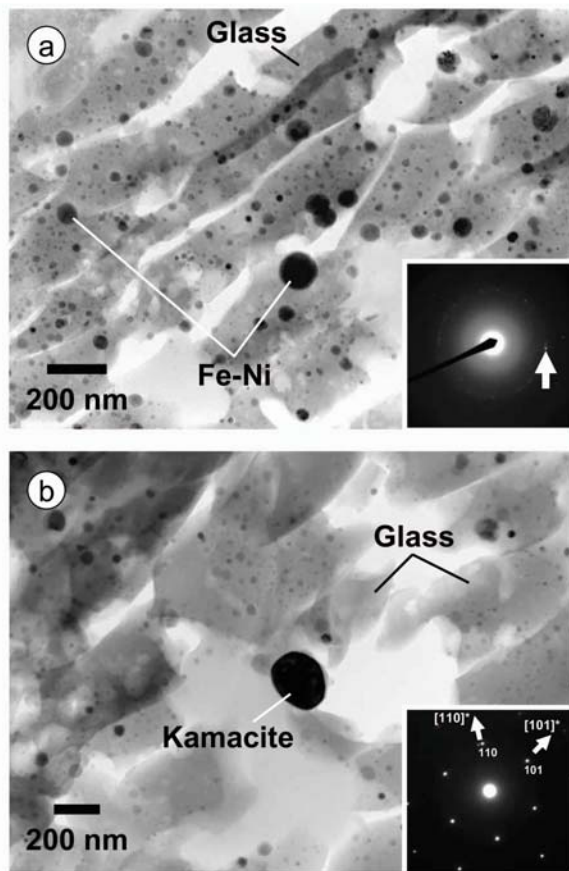
Fig. 14. a) TEM image of a portion of an aggregate of Sample C2004-1-44-4-4 containing a high density of Fe-Ni droplets. On the background are Mg-Fe-bearing Si-O glass (Glass) plates. In the inset is an SAED pattern from an area with high concentration of inclusions showing a diffraction ring at $d = 0.20$ nm (arrow), which corresponds to the strongest (110) reflection of kamacite. b) Image of a relatively large kamacite grain with its SAED pattern (inset).

reflecting the temperature gradient from inside to outside of the particle produced during capture heating.

The Origin of Si-O Glass-Rich Samples

The Mg-Fe-bearing Si-O-rich glass in the four Si-O glass-rich samples, C2004-1-44-4-4, C2054-0-35-16-6, C2054-0-35-44-3, and C2054-0-35-53-3, corresponds to the "glassy silicate bodies" that were found along most tracks in the Stardust aerogel capture cells (Zolensky, personal communication) (e.g., compare Fig. 13 with Fig. 1a in Zolensky et al. [2006]). These "glassy silicate bodies" have received special attention because of their similarity to the glass with embedded metal and sulfides (GEMS) that are common in anhydrous IDPs (Bradley 1994; Zolensky et al. 2006). GEMS are regarded as being among the most primitive solar system materials that may have been amorphized as a result of ionizing irradiation in the interstellar environment before accretion to their parent bodies (Bradley 1994).

It is significant that the four Si-O glass-rich samples exhibit striking similarities in their texture and mineralogy to the inner rim of Sample C2027-2-69-1-4 (compare Figs. 12a and 12b with Fig. 13). These similarities suggest that the four Si-O glass–rich samples were formed by mixing of melted cometary silicates and aerogel during capture heating. The heterogeneities in the Mg, Fe, Ca, and Al contents in the Si-O glass may be related to the distribution of olivine and pyroxene fragments incorporated before melting. The Fe-Ni sulfide/metal droplets were probably produced by melting of the Fe-Ni sulfide and metal carried with the cometary silicates. Therefore, we conclude that the four Si-O glass–rich samples are secondary products formed by interaction between the melted cometary particles and melted aerogel during the capture process.

Fe-Ni-S Inclusions: Relationship to Capture Heating

The Fe-Ni sulfide and metal are contained as small inclusions in two of the three silicate-rich samples (Table 2) and all four Si-O glass-rich samples. They show considerable variation in relative abundance and composition between the samples (Figs. 6a and 6b). This variation gives us an insight into the effects of capture heating.

As mentioned earlier, the Fe-Ni sulfide grains in the silicate-rich Sample FC13-0-17-1-3 probably escaped significant modification. In comparison, the inner rim of the silicate-rich Sample C2027-2-69-1-4 contains not only Fe-Ni sulfide but also sulfide that has apparently been melted and mixed with metal (Fig. 6a), indicating a partial loss of S. The Fe-Ni sulfide/metal inclusions in the Si-O glass-rich Samples C2054-0-35-44-3 and C2054-0-35-53-3 have characteristics similar to those in the inner rim of Sample C2027-2-69-1-4, suggesting that the two samples and the inner rim experienced a similar degree of heating. In contrast, the Fe-Ni-S inclusions in the Si-O glass-rich Sample C2054-0-35-16-6 contain variable amounts of more Ni-rich metal (taenite), and their analyses are plotted widely in the FeS-Fe-FeNi triangle area shown in Fig. 6b. We infer that the analyses reflect a partial loss of S from the more Ni-rich sulfide, probably pentlandite, and that the degree of heating is comparable to that of the other two samples from the same track, Track 35. Compared with the inclusions in these five samples, the inclusions in Sample C2004-1-44-4-4 contain much higher proportions of kamacite (Fig. 6b), suggesting that this sample has been more strongly heated than the other samples.

Editorial Handling—Dr. Scott Sandford

REFERENCES

Ashworth J. R. and Barber D. J. 1975. Electron petrography of shock-deformed olivine in stony meteorites. *Earth and Planetary Science Letters* 27:43–50.

Ashworth J. R. 1985. Transmission electron microscopy of L-group chondrites, 1. Natural shock effects. *Earth and Planetary Science Letters* 73:17–32.

Bradley J. P. 1994. Chemically anomalous, preaccretionally irradiated grains in interplanetary dust from comets. *Science* 265:925–929.

Brearley A. J. and Jones R. H. 1998. Chondritic meteorites. In *Planetary materials*, edited by Papike J. J. Washington, D.C.: Mineralogical Society of America. 398 p.

Brownlee D., Hörz F., Newburn R. L., Zolensky M. E., Duxbury T. C., Sandford S., Sekanina Z., Tsou P., Hanner M. S., Clark B. C., Green S. F., and Kissel J. 2004. Surface of young Jupiter family comet 81P/Wild 2: View from the Stardust spacecraft. *Science* 304:1764–1769.

Brownlee D., Tsou P., Aléon J., Alexander C. M. O'D., Araki T., Bajt S., Baratta G. A., Bastien R., Bland P., Bleuet P., Borg J., Bradley J. P., Brearley A., Brenker F., Brennan S., Bridges J. C., Browning N. D., Brucato J. R., Bullock E., Burchell M. J., Busemann H., Butterworth A., Chaussidon M., Cheuvront A., Chi M., Cintala M. J., Clark B. C., Clemett S. J., Cody G., Colangeli L., Cooper G., Cordier P., Daghlian C., Dai Z., D'Hendecourt L., Djouadi Z., Dominguez G., Duxbury T., Dworkin J. P., Ebel D. S., Economou T. E., Fakra S., Fairey S. A. J., Fallon S., Ferrini G., Ferroir T., Fleckenstein H., Floss C., Flynn G., Franchi I. A., Fries M., Gainsforth Z., Gallien J.-P., Genge M., Gilles M. K., Gillet Ph., Gilmour J., Glavin D. P., Gounelle M., Grady M. M., Graham G. A., Grant P. G., Green S. F., Grossemy F., Grossman L., Grossman J. N., Guan Y., Hagiya K., Harvey R., Heck P., Herzog G. F., Hoppe P., Hörz F., Huth J., Hutcheon I. D., Ignatyev K., Ishii H., Ito M., Jacob D., Jacobsen C., Jacobsen S., Jones S., Joswiak D., Jurewicz A., Kearsley A. T., Keller L. P., Khodja H., Kilcoyne A. L. D., Kissel J., Krot A., Langenhorst F., Lanzirotti A., Le L., Leshin L. A., Leitner J., Lemelle L., Leroux H., Liu M.-C., Luening K., Lyon I., MacPherson G., Marcus M. A., Marhas K., Marty B., Matrajt G., McKeegan K., Meibom A., Mennella V., Messenger K., Messenger S., Mikouchi T., Mostefaoui S., Nakamura T., Nakano T., Newville M., Nittler L. R., Ohnishi I., Ohsumi K., Okudaira K., Papanastassiou D. A., Palma R., Palumbo M. E., Pepin R. O., Perkins D., Perronnet M., Pianetta P., Rao W., Rietmeijer F. J. M., Robert F., Rost D., Rotundi A., Ryan R., Sandford S. A., Schwandt C. S., See T. H., Schlutter D., Sheffield-Parker J., Simionovici A., Simon S., Sitnitsky I., Snead C. J., Spencer M. K., Stadermann F. J., Steele A., Stephan T., Stroud R., Susini J., Sutton S. R., Suzuki Y., Taheri M., Taylor S., Teslich N., Tomeoka K., Tomioka N., Toppani A., Trigo-Rodríguez J. M., Troadec D., Tsuchiyama A., Tuzzolino A. J., Tyliszczak T., Uesugi K.,

Velbel M., Vellenga J., Vicenzi E., Vincze L., Warren J., Weber I., Weisberg M., Westphal A. J., Wirick S., Wooden D., Wopenka B., Wozniakiewicz P., Wright I., Yabuta H., Yano H., Young E. D., Zare R. N., Zega T., Ziegler K., Zimmermann L., Zinner E., and Zolensky M. 2006. Comet 81P/Wild 2 under a microscope. *Science* 314:1711–1716.

Huebner J. S. and Turnock A. C. 1980. The melting relations at 1 bar of pyroxenes composed largely of Ca-, Mg-, and Fe-bearing components. *American Mineralogist* 65:225–271.

Jiang D., Fujino K., Tomioka N., Hosoya T., and Das K. 2002. High-temperature X-ray diffraction study of enstatite up to the melting point. *Journal of Mineralogical and Petrological Sciences* 97: 20–31.

Jones R. H. and Scott E. R. D. 1989. Petrology and thermal history of type IA chondrules in the Semarkona (LL3.0) chondrite. Proceedings of the 19th Lunar and Planetary Science Conference. pp. 523–536.

Jones R. H. 1990. Petrology and mineralogy of Type II, FeO-rich chondrules in Semarkona (LL3.0): Origin by closed-system fractional crystallization, with evidence for supercooling. *Geochimica et Cosmochimica Acta* 54:1785–1802.

Joreau P., Leroux H., and Doukhan J. C. 1997. A transmission electron microscope investigation of shock metamorphism in olivine of the Ilafegh 013 chondrite. *Meteoritics & Planetary Science* 32:309–316.

Kitazawa Y., Fujiwara A., Kadono T., Imagawa K., Okada Y., and Uematsu K. 1999. Hypervelocity impact experiments on aerogel dust collector. *Journal of Geophysical Research* 104:22035–22052.

Kullerud G. 1963. The Fe-Ni-S system. *Carnegie Institution of Washington Year Book*: 62:175–189.

Langenhorst F., Joreau P., and Doukhan J. C. 1995. Thermal and shock metamorphism of the Tenham chondrite: A TEM examination. *Geochimica et Cosmochimica Acta* 59:1835–1845.

Nakamura T., Tomeoka K., and Takeda H. 1992. Shock effects of the Leoville CV carbonaceous chondrite: A transmission electron microscope study. *Earth and Planetary Science Letters* 114:159–170.

Sears D. W., Ashworth J. R., Broadbent C. P., and Bevan A. W. R. 1984. Studies of an artificially shock-loaded H group chondrite. *Geochimica et Cosmochimica Acta* 48:343–360.

Smyth J. R. 1974. Experimental study on the polymorphism of enstatite. *American Mineralogist* 59:345–352.

Tomeoka K. and Itoh D. 2004. Sodium-metasomatism in chondrules in CO3 chondrites: Relationship to parent body thermal metamorphism. *Meteoritics & Planetary Science* 39: 1359–1373.

Zolensky M. E., Zega T. J., Yano H., Wirick S., Westphal A. J., Weisberg M. K., Weber I., Warren J. L., Velbel M. A., Tsuchiyama A., Tsou P., Toppani A., Tomioka N., Tomeoka K., Teslich N., Taheri M., Susini J., Stroud R., Stephan T., Stadermann F. J., Snead C. J., Simon S. B., Simionovici A., See T. H., Robert F., Rietmeijer F. J. M., Rao W., Perronnet M. C., Papanastassiou D. A., Okudaira K., Ohsumi K., Ohnishi I., Nakamura-Messenger K., Nakamura T., Mostefaoui S., Mikouchi T., Meibom A., Matrajt G., Marcus M. A., Leroux H., Lemelle L., Le L., Lanzirotti A., Langenhorst F., Krot A. N., Keller L. P., Kearsley A. T., Joswiak D., Jacob D., Ishii H., Harvey R., Hagiya K., Grossman L., Grossman J. N., Graham G. A., Gounelle M., Gillet Ph., Genge M. J., Flynn G., Ferroir T., Fallon S., Ebel D. S., Dai Z. R., Cordier P., Clark B., Chi M., Butterworth A. L., Brownlee D. E., Bridges J. C., Brennan S., Brearley A., Bradley J. P., Bleuet P., Bland P. A., and Bastien R. 2006. Mineralogy and petrology of comet 81P/Wild 2 nucleus samples. *Science* 314:1735–1739.

APPENDIX

Nondefinable Particles and an Unusual Aggregate in a Silicate-Rich Particle

Samples FC4-0-3-1-1 and FC12-0-16-1 are very different in their mineralogy from the two groups above, and thus are treated as nondefinable samples. In addition, we describe an unusual aggregate found separately from the major aggregates in the silicate-rich Sample C2027-2-69-1-4. Because these two samples and aggregate contain materials that are extremely rare in chondrites and IDPs, they may have been contaminated.

FC4-0-3-1-1

These aggregates on the TEM grid consist mainly of fine grains of Si-O glass (1-100 nm) containing minor, variable amounts of Mg, Al, Ca, and Cl. The aggregates include a variety of materials: 1) an amorphous Al-Zr-O material (Fig. A1a), 2) an amorphous Si-Ca-Mg-Al-O material, and 3) a crystalline Si-O phase, and (4) a crystalline Ti-O phase (Fig. A1b), approximately in the order of abundance. The Al-Zr-O material occurs as rounded to rectangular grains (50 to 400 nm in diameter) having numerous vesicles (1–50 nm in diameter) (Fig. A1a). The grains contain minor variable amounts of S, Zn, and Si. During the TEM observations, vesiculation took place in the grains, suggesting that this material contains volatile material. The Si-Ca-Mg-Al-O material occurs as a single spherical grain (~250 nm in diameter) and smaller anhedral grains; this material is compositionally similar to Ca-Mg-Al pyroxene, although it is amorphous. The Si-O phase occurs as a single angular grain (~200 nm in size). The Ti-O phase occurs as a rounded grain (~130 nm in diameter) (Fig. A1b); from its SAED patterns, it is probably rutile (TiO_2).

Other minor constituents are: (1) a crystalline K-Al-Si-O phase, (2) a crystalline Ca-C-O phase, and (3) a crystalline Fe-O phase. The Ca-C-O phase occurs as grains <30 nm in diameter. This phase is likely to be Ca-carbonate. The Fe-O phase occurs as a grain ~50 nm in diameter, and is the only Fe-rich material found in this sample.

FC12-0-16-1-6

The aggregate on the TEM grid consists of an angular grain of Si-O glass (~2 μm in size) and fine fibrous grains of Si-O glass (150–600 nm in size); no other elements were detected from these grains. No other materials were found in this sample.

The Aggregate of Zn Phase and Ca-C-O Phase in Sample C2027-2-69-1-4

An unusual aggregate (1.5 × 5.5 μm in size) in Sample C2027-2-69-1-4 consists of grains of a Zn phase (100–300 nm in size) and a Ca-C-O phase (100–400 nm) embedded in Si-O glass (Fig. A1c). The Zn phase is crystalline and contains no
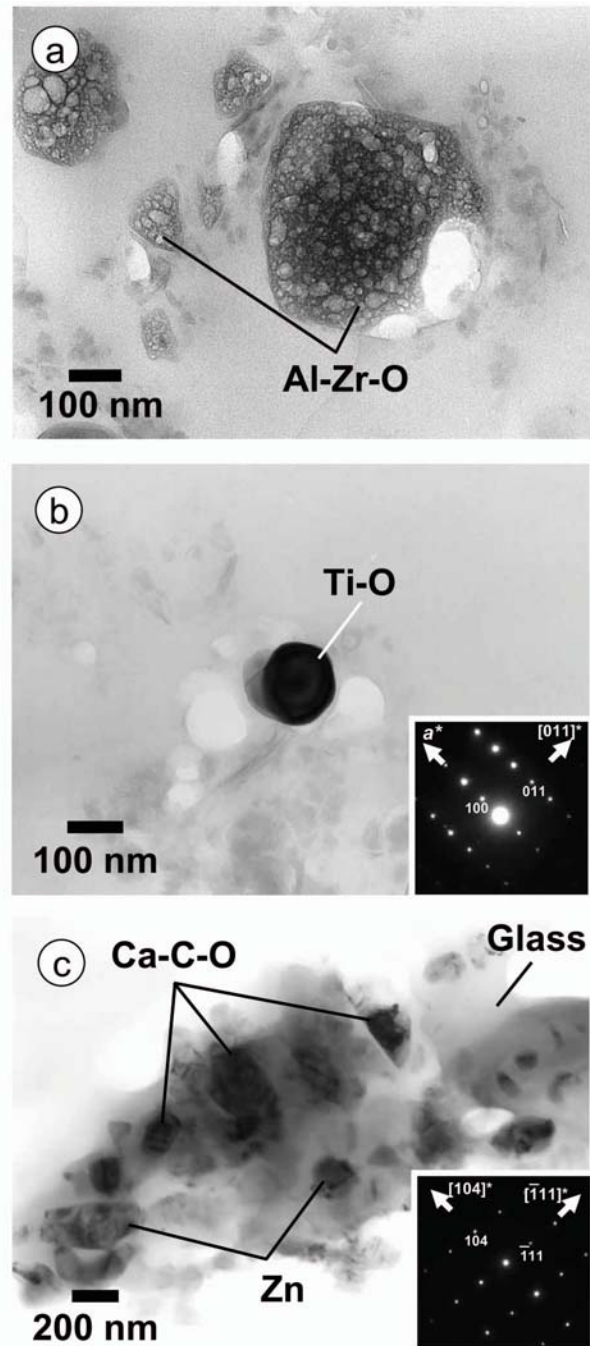

Fig. A1. a) TEM image of grains of the Al-Zr-O material in Sample FC4-0-3-1-1 having numerous vesicles. b) Image of a Ti-O grain in Sample FC4-0-3-1-1 and its SAED pattern (inset), which is consistent with rutile. c) Image of an aggregate of grains of Zn phase and Ca-C-O phase embedded in Si-O glass in Sample C2027-2-69-1-4. In the inset is an SAED pattern from a Ca-C-O grain, which is consistent with calcite.

significant amounts of any other elements. This phase may be metal, but it could not be identified using electron diffraction. From the SAED patterns, the Ca-C-O phase is probably calcite. The Si-O glass contains minor amounts of Cl.